Histogram Maximum Value Index Based Nano-scale Particle Classification

Kapila K. Pahalawatta
Computer Science and Software Engineering
University of Canterbury
Christchurch, New Zealand
kkp17@uclive.ac.nz

Richard Green
Computer Science and Software Engineering
University of Canterbury
Christchurch, New Zealand
richard.green@canterbury.ac.nz

Abstract—In the current study, two proposed histogram maximum value index (MVI) based classification methods are introduced and compared for classifying five different sized airborne nano-scale particles. Method-I uses the histogram MVIs of separate single channelled (red, green and blue) images and MVIs of 4-dimensional complete RGB colour histograms are used by the method-II. Taking into account the selective colour scattering behaviour of the Rayleigh scattering phenomenon, red, green and blue intensities of the scattered light of a continuous spectrum of light by the particles are investigated using the colour histograms of captured video images. Running mode and running mean of histogram MVI over a window of fixed number of frames (N) are used to construct the feature vectors for particle discrimination. Both methods failed to classify wood smoke correctly due to its complex composition of many types of monotype particles. However, method-II classified all the monotype smoke particles correctly with 100% accuracy when N≥90 and the number of histogram bins=256x256x256. Method-I was faster and also achieved the same accuracy when N≥100 and the number of bins in each red, green and blue histograms = 256.

Keywords-Particle classification, colour histogram, histogram maximum value index, Rayleigh scattering

I.   INTRODUCTION

The RGB colour histogram of an image with N pixels is defined by the following probability mass density function of the image intensities.

$$h_{R,G,B}(a.b.c)=N.\mathrm{Prob}(R=r,\ G=g,\ B=b) \qquad (1)$$

where, R, G and B are the three colour (red, green and blue) channels.

The histogram of a single channelled image (or intensity histogram) is defined as

$$h_A\ (a)=N.\mathrm{Prob}(A=a) \qquad (2)$$

where, A is the selected colour (R, G or B) channel. In both (1) and (2) r, g, b and a can get any value between 0 and 255.

The main difficulty with RGB colour histogram based retrieval is histogram high dimensionality, even with drastic quantizations of the colour space. In contrast to colour histograms, it is computationally inexpensive to work with the three single R, G and B channelled image histograms even though, they are less informative.

In an intensity histogram, if

$$h_A\ (X) = \max\{\ h_A\ (a)|\ a\ \epsilon\ [0,255]\},$$

X can be defined as the Maximum Value Index (MVI) of the intensity histogram. In contrast to the singleton MVI of an intensity histogram, the MVI of a colour histogram is expressed by the triplet (X, Y, Z) where

$$h_{R,G,B}(X, Y, Z) = \max\{h_{R,G,B}(a,b.c)|\ a,\ b,\ c\ \epsilon\ [0,255]\}.$$

In prior literature, comparisons of histogram bin values were extensively used in colour histogram based image classifications [1, 2 and 3]. In the case of images of airborne nano-scale particles, this signature becomes quite ineffective due to the high variability of particle density and the overlapping of these pixel sized objects in comparing images. By analysing the image histograms of consecutive video frames, it was discovered that the MVI of the histogram is a particle density independent feature and in this study six image signatures based on intensity and colour histogram MVIs are used for classification. For clarity, the notation $MVI_{k,l}$ is used to identify these signatures. In this notation k is the histogram type (either intensity or colour) and l is the selected channel (R, G or B). For example, $MVI_{Intensity,\ G}$ is the histogram MVI of the constructed "green" channel image. $MVI_{Colour,\ G}$ is the green value of the colour histogram MVI of the colour image (value of the second element of the tuple).

When a particle size is less than one tenth of the incident wavelength, the visibility of that particle is mostly explained by the Rayleigh scattering theory and, if the particle size is greater than the incident wavelength, then its visibility is explained by Mie scattering theory [4, 5 and 6].

The following equation explains the Rayleigh scattering by a single particle [6].

$$I(\theta) = I_0 \frac{1+\cos^2\theta}{2R^2}\left(\frac{2\pi}{\lambda}\right)^4\left(\frac{n^2-1}{n^2+2}\right)^2\left(\frac{d}{2}\right)^6 \qquad (3)$$

where, $I(\theta)$ is the scattered light intensity by the particle at angle θ,

θ is the scattering angle

R is the distance to the particle

I_0 is the intensity of incident light

n is the refractive index of the particle

λ is the wavelength of incident light and

d is the diameter of the particle.

The intensity of Rayleigh scattered light is proportional to the sixth power of the particle size and inversely proportional to the fourth power of the incident wavelength. Therefore, for particles of same size, shorter-wavelength-light will be scattered with a higher visible intensity than the longer-wavelength-light (e.g. blue light with wavelength 460 nm will be scattered four times more than the red light with wavelength 650 nm). On the other hand, the same incident light will be scattered in different intensities by different sized particles.

In the present classification method, this selective light scattering behaviour of the Rayleigh scattering phenomenon is used to classify five different sized particles (kerosene smoke, polyurethane smoke, cooking oil smoke, water steam and wood smoke). The intensities of scattered red, green and blue components of a continuous spectrum of light (a white LED light with wavelengths ranging from 400 nm to 800 nm) by these particles (particle diameters ranging from 40 nm to 300 nm [7]) is analysed using histogram MVI values.

II.   RELATED WORK

Using an infrared laser light (wavelength λ=780 nm) as the light source, Li *et al.* [2] successfully classified three different types of particles (Kerosene smoke, cigarette smoke and water vapour) with the rate of discrimination at about 95%. In their study, the output signal of a silicon photoreceptor was used to measure the intensity of the Mie scattered infrared laser light.

<<Other than this work, all the other large number of studies haves been carried out to detect airborne particles in open environments using surveillance cameras with extensive use of noise filters to eliminate the unnecessary environmental noise. >>All this prior research is based on the extraction and analysis of behavioural characters and features of smoke cloud and none of them addressed the issue of classifying individual particles by extracting the individual particle characters. Motion [8, 9, 10, 11], texture [9], edge detection [8, 9, 12], region analysis [9], colour information [8, 9, 10, 13], disorder, frequent flicker in boundaries, self similarity and local wavelet energy [11], shape variation or growth [11, 13] are some of the extracted features and behavioural characters of smoke clouds in these studies. The classifications were carried out merely for distinguishing the smoke clouds from other non-hazardous image features such as changing in background lighting and moving vehicles and not for classifying types of hazardous smoke from non-hazardous air-borne particles. None of this prior research computed a clear quantifiable measure to enable comparing the classification efficiency and the accuracy of their work with other studies.

III.   CLASSIFICATION PROCESS

The steps of the proposed classification process in this research; background preparation and illumination, image capturing, smoke pixel isolation, image preparation and visual feature extraction, construction of feature vectors, particle classification, analysis of results and comparison are explained in detail in this section.

A.   Background Preparation and Illumination

A closed particle chamber which resembles the smoke chamber in a common photoelectric smoke detector with a white background was used. To avoid the changes in intensity due to the outside light sources, all the images were captured inside the chamber. To maintain an even particle density inside the chamber a small electric fan was continuously operated inside the chamber.

To illuminate the chamber, a phosphor-based white LED which covers a spectrum from 400 nm to 800 nm of wavelength light was used. Figure 1 shows the spectrum (relative luminous intensity vs. wavelength) of this LED.
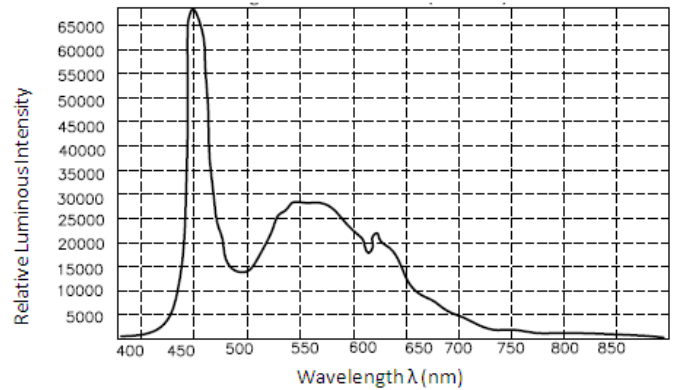

Figure 1.   Spectrum of the used white LED (from SPC Technology technical datasheet, MC20358).

B.   Image Capturing

All the colour videos were captured using a USB digital microscope magnification up to 200X and a resolution 640 x 480 pixels.

C.   Construction of "Noise-only" Image With Modified Frame-difference Method (Smoke Isolation)

If I_{t_n} is an image of the frame n which is taken at time t_n, the pixel value s located at x at time t_n in the difference image is defined as

$$s(t_n, x) = | p(I_{t_n}, x) - p(I_{t_{n-1}}, x) | \qquad (4)$$

where, $p(I_t, x)$ is the pixel value at x in the image I_t.

Let k be the number of frames before the particle cloud was introduced. Then the noise pixels in the nth $(n > k)$ affected image can be identified by the difference image between $I_{t_n} (n > k)$ and one of the non-affected images $I_{t_m} (m \geq k)$.

By modifying (4), the pixel value d located at x at time t_n in the difference image of these affected and non-affected images can be defined as

$$d(t_n, x) = |\ p(I_{t_n}, x) - p(I_{t_m}, x)\ | \qquad (5)$$

where, $m \in [1, k]$ and $n \in]k, N]$ and N is the total number of frames.

A thresholded difference image was used to construct the "noise-only image" and the pixel value n located at x at time t_n in the noise-only image was calculated as

$$\mathbf{n}(t_n, \mathbf{x}) = \begin{cases} p(I_{t_n}, \mathbf{x}) \ for \ \mathbf{d}(t_n, \mathbf{x}) \geq T \\[1em] 0 \qquad for \ \mathbf{d}(t_n, \mathbf{x}) < T \end{cases} \qquad (6)$$

D. Image Preparation And Visual Feature Extraction

Colour and single channelled (separate red, green and blue) noise-only images were used to extract the features. Each image of the captured colour video sequence was divided into its red, green and blue single-channel images. Noise-only images were constructed for both the colour images and its three single channelled images according to (4).
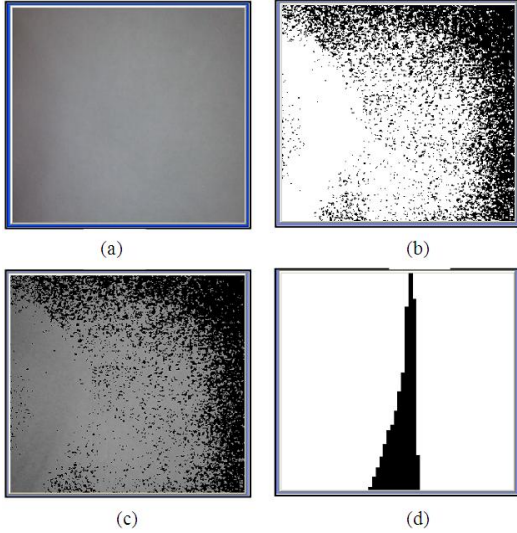

Figure 2. An image of kerosene smoke particles (a), thresholded difference image (b), the noise-only (extracted smoke pixels) image (c) and "Green" channel noise intensity histogram (d) of image (c).

Noise intensity histogram, the MVI and, running mean, mode and standard deviation of MVI over a window of fixed number of frames (50, 100, 150 and 200) were calculated for all four noise-only images (colour and three single channelled) of each image in all particle video frame sequences.

For example, the thresholded difference image (fig. 2(b)) using (5), noise-only image (fig. 2(c)) using (6) with the corresponding intensity histogram of smoke pixels of "green" channel (fig. 2(d))of a kerosene smoke image (fig. 2(a)) is shown in figure 2.

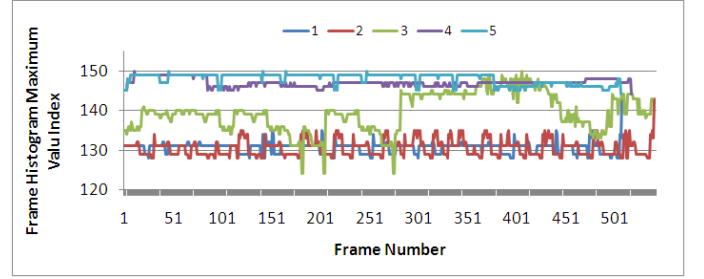The variation of $MVI_{Intensity,G}$ of all particles over 500 frames is shown in figure 3.

Figure 3. The variation of $MVI_{Intensity,G}$ for all particles (1- polyurethane; 2- kerosene; 3- wood; 4- steam; 5- oil) over 500 frames.

The variation of running averages of $MVI_{Intensity,G}$ for all particles (in figure 3) with a window of hundred frames is shown in figure 4(a) with the running averages of $MVI_{Colour,G}$ shown for all particles in figure 4(b) for comparison. With the window size 100, running modes of $MVI_{Intensity,R}$, $MVI_{Colour,R}$, $MVI_{Intensity,G}$, $MVI_{Colour,G}$, $MVI_{Intensity,B}$, $MVI_{Colour,B}$ for all particles (1- polyurethane; 2- kerosene; 3- wood; 4- steam; 5- oil) are shown in figures 4(c), 4(d), 4(e), 4(f), 4(g) and 4(h) respectively.

E. Construction of Feature Vectors

The extracted nine features of single channelled images (running means, modes and standard deviations of $MVI_{Intensity, R}$, $MVI_{Intensity, G}$ and $MVI_{Intensity, B}$) and the extracted nine features of colour images (running means, modes and standard deviations of $MVI_{Colour, R}$, $MVI_{Colour, G}$ and $MVI_{Colour, B}$) were used to build the different feature vectors for method-I and method-II respectively.

F. Particle Classification

A half of the total number of windows of each particle sequence was used as the training data and the other half was used as the test data. For example, 200 training data sets and 200 test data sets from each particle type prepared 1000 training data sets and 1000 test data sets when the moving window size (N) is 100. A widely used classification algorithm, K-nearest neighbour algorithm [14, 15, and 16] was used and the classification is based on collection of pre-stored data.

IV. RESULTS AND DISCUSSION

Total number of test instances, total number and the total number as a percentage of correctly identified instances by Method-I (with 256 histogram bins for each channel) and Method-II (with 256x256x256 colour histogram bins) for four different window sizes are shown in table-I and table-II respectively. In both tables, correctly identified instances are divided into two categories according to the two used mutually independent feature vectors; feature vectors constructed with mean and standard deviation and the feature vectors constructed with mode, for classification. Both test and training instances consists of feature vectors from all five particles.
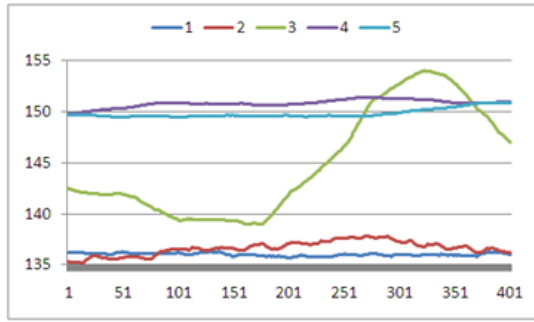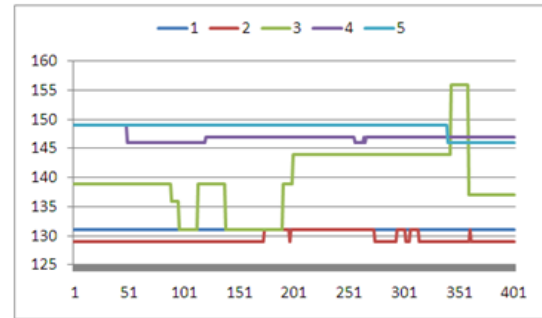
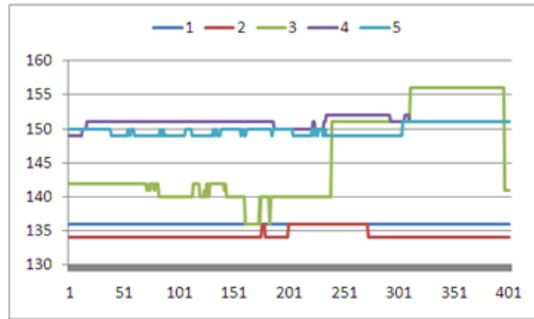**(a)** Running averages of $MVI_{Intensity, G}$ of first 400 windows of all particles with window size 100.
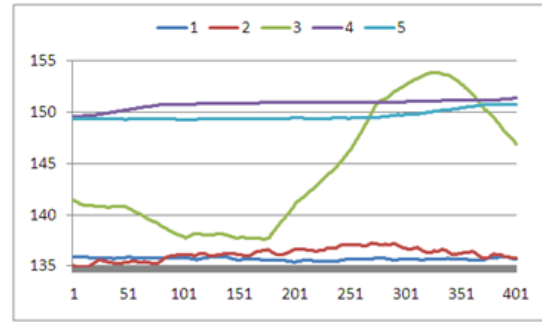
(b) Running averages of $MVI_{Colour, G}$ of first 400 windows of all particles with window size 100.
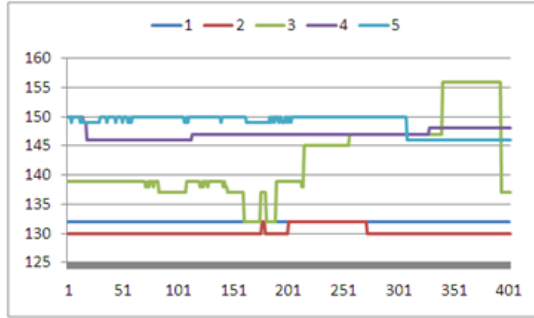
(c) Running modes of $MVI_{Intensity, R}$ of first 400 windows of all particles with window size 100.

(d) Running modes of $MVI_{Colour, R}$ of first 400 windows of all particles with window size 100.

(e) Running modes of $MVI_{Intensity, G}$ of first 400 windows of all particles with window size 100.

(f) Running modes of $MVI_{Colour, G}$ of first 400 windows of all particles with window size 100.
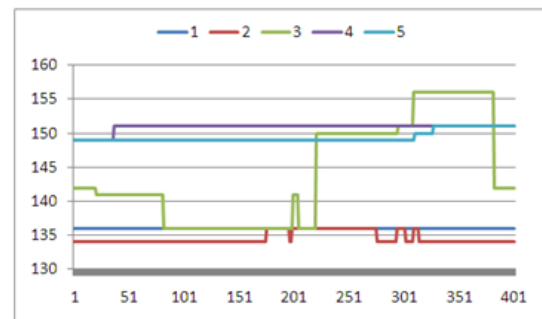
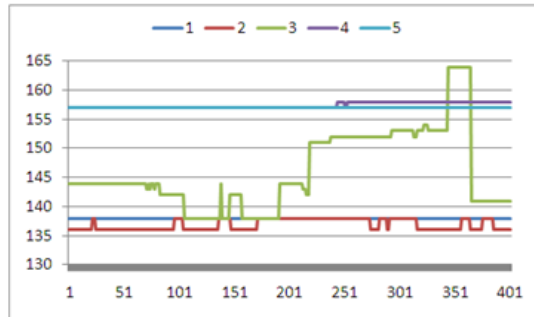**(g)** Running modes of $MVI_{Intensity, B}$ of first 400 windows of all particles with window size 100.

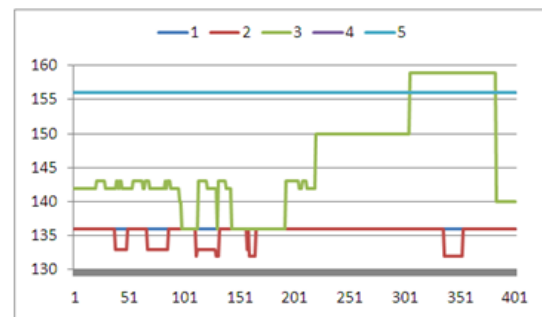**(h)** Running modes of $MVI_{Colour, B}$ of first 400 windows of all particles with window size 100.

Figure 4. The variation running modes and running averages of MVIs (1- polyurethane; 2- kerosene; 3- wood; 4- steam; 5- oil)

TABLE I.   CLASSIFICATION RESULTS OF ALL THE FIVE DIFFERENT PARTICLES WITH METHOD-I (K=10).

Window size	Test Instances	Correctly Identified Instances			
		With mean and Standard deviation		With Mode	
		Instances	%	Instances	%
50	1125	854	75.92	869	77.24
100	1000	810	81	818	81.80
150	875	734	83.89	745	85.14
200	750	632	84.27	654	87.20

TABLE II.   CLASSIFICATION RESULTS OF ALL THE FIVE DIFFERENT PARTICLES WITH METHOD-II (K=10).

Window size	Test Instances	Correctly Identified Instances			
		With mean and Standard deviation		With Mode	
		Instances	%	Instances	%
50	1125	863	76.71	870	77.33
100	1000	819	81.90	825	82.50
150	875	752	85.94	772	88.23
200	750	661	88.13	672	89.60

As illustrated in figure 3 (here, variation of only $MVI_{Intensity,G}$ is illustrated as an example, but all other five MVIs have the similar patterns of variations), in most frames, each MVI tends to stay in a fixed value rather than varying randomly around its average. Therefore, less fluctuating more separable feature vectors can be obtained with signatures with mode values rather than signatures with means and standard deviations (compare the fig. 4(a) 4(b) with 4 (d) and 4(e)) and this is clarified by the results of table I and II. Again, increasing the size of the moving window also results in less fluctuations of running means and modes. For example, the variation of running modes with window size 50 and 200 for R layer kerosene data is shown in figure 4.
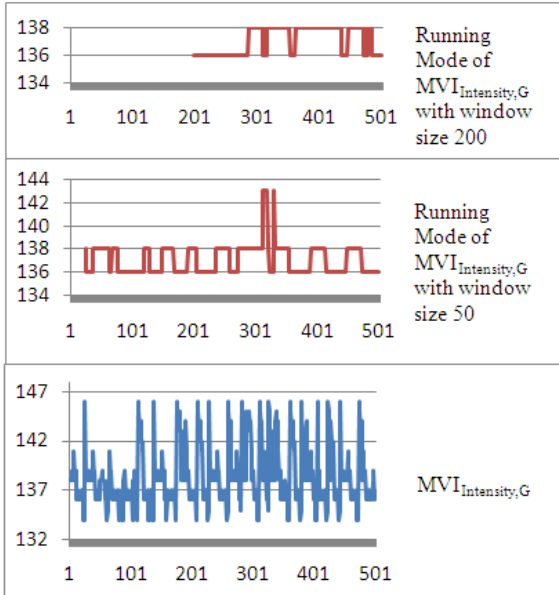

Figure 5.   Running mode of $MVI_{Intensity,\ G}$ with window size 50 and 200 for R layer kerosene data.

In both methods, due to the wide fluctuation of the running means and modes of wood smoke particles, most of the incorrectly identified instances were classified as wood smoke particles because the K-nearest neighbour algorithm always classifies test instances according to their closest neighbours (in this case, wood training instances).

After removing both test and training instances of wood smoke, the classification results with all other monotype particles (polyurethane smoke, kerosene smoke, water vapour and oil smoke) are shown in table III and IV.

TABLE III.   CLASSIFICATION RESULTS OF ALL FOUR MONOTYPE PARTICLES WITH METHOD-I (K=10).

Window size	Test Instances	Correctly Identified Instances			
		With mean and Standard deviation		With Mode	
		Instances	%	Instances	%
50	900	845	93.9	863	95.89
90	980	935	95.41	958	97.76
100	800	800	100	800	100.00
150	700	700	100	700	100.00
200	600	600	100	600	100.00

TABLE IV.   CLASSIFICATION RESULTS OF ALL FOUR MONOTYPE PARTICLES WITH METHOD-II (K=10).

Window size	Test Instances	Correctly Identified Instances			
		With mean and Standard deviation		With Mode	
		Instances	%	Instances	%
50	900	862	95.78	876	97.33
90	980	968	98.78	980	100.00
100	800	800	100.00	800	100.00
150	700	700	100.00	700	100.00
200	600	600	100.00	600	100.00

V. CONCLUSION

The results show that the proposed colour and red, green and blue single channeled histogram MVI's of monotype nano-scale particle images which were generated by Rayleigh scattered light can be used to classify those particles accurately. Furthermore, the variation of MVI can be used as a measure of purity of the particle cloud since its mode, mean and standard deviation varies widely and rapidly with particle clouds of more than one type.

Although, both methods proposed in this paper identified all the monotype particle clouds (kerosene smoke, polyurethane smoke, water steam and cooking oil smoke) with 100% accuracy, Method-II achieved that accuracy with window size of 90 frames in contrast to 100 frames in Method-I. However, Method-I was significantly faster, even with 3x256 intensity histogram bins (red, green and blue) compared to the 256x256x256 colour histogram bins in Method-II.

REFERENCES

[1] S. Sergyan, "Color histogram features based image classification in content-based image retrieval systems", *6th IEEE International Symposium on Applied Machine Intelligence and Informatics*, pp. 221-224, 2008.

[2] Z. Zhang, W. Li, B. Li, "An Improving Technique of Color Histogram in Segmentation-based Image Retrieval", *Fifth IEEE International Conference on Information Assurance and Security*, Vol.2, pp. 381-384, 2009.

[3] G.R. Bradski, A. Kaehler, "Learning OpenCV: Computer Vision with the OpenCV Library", Sebastopol, CA : O'Reilly, 2008.

[4] Wikipedia, The free encyclopaedia, http://en.wikipedia.org/wiki/Rayleigh_scattering, visited on 15/10/2011.

[5] J. Li, S. Wang, Z. Dou and Z. Yang, "Discrimination of Smoke Particles Using Infrared Photoelectrical Detection", *International journal of Infrared and Millimetre Waves,* vol. 22, No. 1, pp. 141-151, 2001.

[6] N. S. Kopeika, "A system engineering approach to imaging", SPIE Optical Engineering Press, Bellingham, pp. 446-451, 1998.

[7] T. Z. Fabian, P. D. Gandhi, Smoke Characterization Project, Technical report, Underwriter Laboratories Inc, Northbrook, IL 60062, 2007.

[8] D. Han, B. Lee, "Development of Early Tunnel Fire Detection Algorithm using the Image Processing", LNCS 4292, pp. 39-48. 2006.

[9] B. Lee, D. Han, "Real-Time Fire Detection Using Camera Sequence Image in Tunnel Environment", *LNCS 4861*, pp. 1209-1220, 2007.

[10] J. Capitan, D. Mantecon, P. Soriano, A. Ollero, "Autonomous perception techniques for urban and industrial fire scenarios", Proceedings of the 2007 IEEE International Workshop on Safety, Security and Rescue Robotics, Rome, Italy, 2007.

[11] Z. Xu, J. Xu, "Automatic Fire Detection Based on Image Visual Features", IEEE International Conference on Computational Intelligence and Security Workshops, pp 316-319, 2007.

[12] V. Cappellini, L. Mattii, A. Mecocci, "An Intelligent System for Automatic Fire Detection in Forests" LNCS 399, pp. 351-364, 1989.

[13] T.-H. Chen, Y.-H. Yin, S.-F. Huang, Y.-T. Ye, "The smoke Detection for Early Fire-Alarming System Base on Video Processing", IEEE proceedings of the International conference on Intelligent Information Hiding and Multimedia Signal Processing, pp. 427-430, 2006.

[14] T. Hastie, R. Tibshirani, J. Friedman, The Elements of Statistical Learning — Data Mining, Interface and Prediction. Canada: Springer, pp. 415-426, 2001.

[15] H.-T. Chen, F.-T. Chen, S. Buthpitiya, Y. Zhang, A. Nefian, "Lunar Image Classification for Terrain Detection", *Silicon Valley Campus.* Paper 18 (http://repository.cmu.edu/silicon_valley/18), 2010.

[16] X.-g. Yu, X.-p. Yu, "Locally Adaptive Text Classification Based K-Nearest Neighbors", *International Conference on Wireless Communications, Networking and Mobile Computing*, pp. 5651 – 5654, 2007.